PCCP

Accepted Manuscript

This is an *Accepted Manuscript*, which has been through the Royal Society of Chemistry peer review process and has been accepted for publication.

Accepted Manuscripts are published online shortly after acceptance, before technical editing, formatting and proof reading. Using this free service, authors can make their results available to the community, in citable form, before we publish the edited article. We will replace this *Accepted Manuscript* with the edited and formatted *Advance Article* as soon as it is available.

You can find more information about *Accepted Manuscripts* in the Information for Authors.

Please note that technical editing may introduce minor changes to the text and/or graphics, which may alter content. The journal's standard Terms & Conditions and the Ethical guidelines still apply. In no event shall the Royal Society of Chemistry be held responsible for any errors or omissions in this *Accepted Manuscript* or any consequences arising from the use of any information it contains.

ROYAL SOCIETY OF CHEMISTRY

www.rsc.org/pccp

Journal Name

ARTICLE

Ni_3S_2@CoS core-shell nano-triangular pyramid arrays on Ni foam for high-performance supercapacitors

Received 00th January 20xx,
Accepted 00th January 20xx

DOI: 10.1039/x0xx00000x

www.rsc.org/

Rui Li, Senlin Wang,[*a] Jianpeng Wang, and Zongchuan Huang

In this paper, we demonstrate a facile method to fabricate a novel Ni_3S_2 nano-triangular pyramid (NTP) arrays on Ni foam though a hydrothermal process and build the unique Ni_3S_2@CoS core-shell NTP arrays by electro-deposition. The obtained Ni_3S_2@CoS material displays twice the specific capacitance for pure Ni_3S_2 material in both the three-electrode system (4.89 F cm^{-2} at 4 mA cm^{-2}) and asymmetric supercapacitor device (0.69 F cm^{-2} at 1.43 mA cm^{-2}). Meanwhile, the asymmetric supercapacitor demonstrates an outstanding energy density of 28.24 Wh kg^{-1} at a power density of 134.46 W kg^{-1}, with a stable cycle life (98.83% retained after 2000 cycles). The unique structure of Ni_3S_2@CoS core-shell NTP arrays, which provides an ultra-thin CoS shell to enlarge efficient areas, introduces good conductivity, short transportation lengths for both ions and electrons, contributes most to its excellent performance. Moreover, the bare Ni_3S_2 NTP arrays can be used as a new template to build other potential electrode materials.

1. Introduction

In the 21th century, it is very urgent to develop new energy resources to meet the global energy crisis. In recent years, researchers have discovered several renewable energy sources such as wind, solar, geothermal and so on. However, these energy sources are unable to work efficiently because of their heavily depending on natural conditions. Supercapacitors, a new practical capacitor, have emerged as feasible alternatives to complement or replace batteries based on advantages of high power density, fast recharge ability and long cycle life.[1-6] According to charging storage mechanism, supercapacitors are generally including electric double layer capacitors (EDLCs) that involve physical absorption/desorption ions between electrode and electrolyte interface and pseudocapacitors that rely on redox reactions occur on the surface of active materials. Compared with EDLCs, pseudocapacitors based on metal oxides/hydroxide and conducting polymers exhibit high specific capacitance because they can provide a variety of oxidation states for charge storage,[7-9] while EDLCs suffer from low specific capacitance and rate capability.[10] Unfortunately, those materials are hindered by their nature. For instance, RuO_2 is too expensive to be a practical option as electrode materials in spite of its high performance,[11] while conducting polymers such as polyaniline is complicated by the demand for proper proton activity in the electrolyte employed in charging and discharging.[12]

Nowadays, metal sulfides have attracted wide attention owe to their intrinsic physical and chemical properties.[13-16] Among them, the heazlewoodite Ni_3S_2 has many advantages for the application of supercapacitors, including good conductivity, natural abundance and versatility.[13, 17, 18] However, the practical application of Ni_3S_2 for supercapacitiors is hindered by low active mass utilization and fast attenuation.[15] In this regard, many efforts have been devoted to overcome these problems, such as increasing the effective contact area of electrode/electrolyte by forming ordered morphology or introducing other materials to build composites. Among these methods, the scalable synthesis of core-shell heterostructures has been provided as a rational and facile strategy to promote the performance of materials for the reason of synergetic effect. Thus, electrochemical performances are improved by taking the advantages of their unique shapes, multifunctionality of each component, and controllability of building primary templates. Although many advanced core-shell materials have been fabricated in previous works,[19-21] core-shell composite based on Ni_3S_2 remains to be explored. For instance, Zhou *et al.* synthesized Ni_3S_2 nanorods/Ni foam electrode via a hydrothermal process.[22] These Ni_3S_2 nanorods were formed in a toxic environment due to the application of poisonous thioacetamide (TAA) as sulfur source and inductive agent. Wei *et al*. demonstrated a Ni_3S_2@NiS composite electrode and obtained serials of composites based on the Ni_3S_2@NiS template by partial ion-exchange.[23] Though the products were endowed with very spectacular performance, the time was long and the step was complicated. Zhou *et al.* coated $Ni(OH)_2$ nanosheets on Ni_3S_2

[a] College of Materials Science & Engineering, Huaqiao University, Xiamen, Fujian, 361021, People's Republic of China. Fax: +86-595-22693746. E-mail address: slwang@hqu.edu.cn

† Electronic Supplementary Information (ESI) available. See DOI: 10.1039/x0xx00000x

nanorods performed a relatively high area specific capacitance (4.7 F cm^{-2} at 2 mV s^{-1}).[24] However, the whole process was sensitive to temperature and time so that the core-shell heterostructure easily got out of control. Till now it is still a great challenge to explore a facile and easy accessibility method to build a Ni_3S_2 template with a rational shell. As a result, we choose an important metal sulfide CoS as the shell of Ni_3S_2 template, which has been widely applied for supercapacitors.[25-27] Although both the Ni_3S_2 and CoS have been extensively reported as electrode materials for supercapacitors, an array heterostructure composed of Ni_3S_2 and CoS hasn't been reported yet.

Herein, we propose a facile method to build novel Ni_3S_2@CoS core-shell NTP arrays on Ni foam with excellent performances for supercapacitors. Especially, this study has the following ideas and contents. (1) Recently Ni_3S_2 has attracted scientists' interests due to its inherent advantages. However, researches were generally hampered by the complex methods, little active materials and toxic environment. In order to solve these problems and make full use of Ni_3S_2, we began to produce a kind of Ni_3S_2 electrode material with hierarchical structure through a facile and green method. (2) It took some time to construct this novel Ni_3S_2 NTP arrays. The critical point of this study was exploring controlled morphology to get the hierarchical Ni_3S_2 NTP arrays. The method of preparation Ni_3S_2 NTP array core is innocuous for the using of thiourea as sulfur source. Additionally, the in-situ growth of the nano-composites on Ni foam can be directly served as an electrode without using of binders and conductive agent. (3) As we expected, the Ni_3S_2@CoS core-shell NTP arrays on Ni foam as a kind of electrode materials have exerted high electrochemical performances. This new core-shell heterostructure is based on synergetic effects of hydrothermal Ni_3S_2 NTP arrays on Ni foam as the core supporter and the electrodeposited CoS shell nanosheets. First, the Ni_3S_2 NTP arrays can be a good conductor to improve electron and ion transfer. Second, the vertical interlaced ultrathin CoS shell can greatly shorten the diffusion pathways of ions. In a word, the unique structure of the composites, which introduces large efficient areas, good conductivity, and short transportation paths for both ions and electrons, contributes most to its excellent performance.

2. Experimental sections

2.1 Materials

The thiourea and $CoCl_2 \cdot 6H_2O$ were purchased from Sinopharm Chemical Reagent Co. Ltd (China). The Ni foam was purchased from CORUN Co. Ltd (China). And the activated carbon (YEC-8A) was purchased from Fuzhou Yihuan Carbon Co. Ltd (China) and its surface area was more than 2100 m^2 g^{-1}. All other regents and materials were analytical grade and used without any further purification.

2.2 Synthesis of Ni_3S_2 NTP arrays on Ni foam

Firstly the Ni foam (1 cm × 1 cm × 1.6 mm) was pretreated with acetone, ethanol and deionized (DI) water to remove oxides from the surface and dried in the oven. Then, the Ni_3S_2 NTP arrays were formed by the sulfuration of Ni foam through a facile hydrothermal reaction. In brief, 0.01 mol thiourea was dissolved in 70 ml mixed solution consisted of DI water and ethanol (volume ratio 4:3) and stirred for 30 minutes continuously. Then the solution was placed in a 100 ml Teflon-lined stainless autoclave with 8 pieces of pretreated Ni foam in it and followed by hydrothermal at 160 °C for 6 h. Other parallel experiments with different temperature (120 °C, 140 °C) were provided in supporting information. After that, the autoclave was naturally cooled down to room temperature and the products were collected by washing with DI water and ethanol. After that the products were dried in the oven. Thus, the Ni_3S_2 NTP arrays on Ni foam were obtained. According to the reaction, the mass of the active Ni_3S_2 material is derived from $m = \Delta m \times (M_{Ni3S2} / 2M_S) = \Delta m \times 240 / 64$. In this equation, Δm represents the weight increment of Ni foam which can be directly weighted after the synthesis of Ni_3S_2 NTP arrays on Ni foam, where M is the molecular weight or atomic weight.[22] The mass loading of Ni_3S_2 on the Ni foam is approximately calculated to be 12 mg.

2.3 Synthesis of Ni_3S_2@CoS core-shell NTP arrays on Ni foam

The Ni_3S_2@CoS core-shell NTP arrays were obtained through an electro-deposition.[28] The experimental was carried out on a CHI 630D electrochemical analyzer with a three-electrode cell, in which Ni_3S_2 NTP arrays on Ni foam, Ag/AgCl and Pt sheet (1 cm × 1 cm) were served as work electrode, reference electrode and counter electrode, respectively. Besides, the electro-deposition bath was composed of 0.5 mmol L^{-1} $CoCl_2 \cdot 6H_2O$ and 0.75 mol L^{-1} thiourea. The whole deposition process was performed by cyclic voltammetry (CV) method for 8 cycles at 5 mv s^{-1} in the voltage range from -1.2 to 0.2 V. Then, the as-prepared sample was washed with DI water and dried in an oven at room temperature for 10 h. Consequently, the Ni_3S_2@CoS core-shell NTP arrays were obtained. The samples were weighed after electrodepositing and the gain weight before and after the deposition is the mass loading of CoS nanosheets. The mass loading of CoS is almost 1.0 mg.

2.4 Characterization

The phases and compositions of samples were estimated by power X-ray diffraction (XRD, Smart lab 3Kw, Japan) with Cu Kα radiation (λ = 1.5418 Å) and energy dispersive spectroscopy (EDS, ISIS-300, Oxford). The micro morphology of samples was characterized by field emission scanning electron microscopy (FESEM, SU8080, Japan) and high resolution transmission electron microscopy (HRTEM, JEM-2100). X-ray photoelectron spectroscopy (XPS) measurements were performed on a VG Escalab MK II spectrometer (Scientific Ltd.) with non-monochromatic Al K X-ray (1486.6 eV). The pressure in the chamber during the experiments was less than 10-6 Pa. The analyzer was operated at 20 eV pass energy with an energy step size of 0.1 eV.

2.5 Electrochemical measurements

The electrochemical behaviours of samples included cyclic voltammetry (CV), galvanostatic charge-discharge and electrochemical impedance spectroscopy (EIS) were detected

on a CHI 660E electrochemical workstation. Briefly, the obtained products were used as a work electrode while Hg/HgO and a Pt sheet (3 cm × 3 cm) were used as the reference electrode and counter electrode with 2 M KOH as electrolyte in a three-electrode cell.

2.6 Fabrication of asymmetric supercapacitor (ASC) devices

The as-prepared samples were used as positive electrode and activated carbon was used as negative electrode to assemble ASC devices in an aqueous 2 M KOH electrolyte. The mass loading of the two electrode materials must be balanceable. The electrochemical performance of the ASC was accomplished by a CHI 660E electrochemical workstation as well. And the long cycle life of ASC devices was inspected through a LAND battery test system (CT2001A).

2.7 Calculations

The capacitances associated with charge-discharge curves could be calculated according to the equation below：

$$C_{\mathrm{a}} = I\Delta t/S\Delta V \quad (1)$$

$$C_{\mathrm{m}} = I\Delta t/m\Delta V \quad (2)$$

where C_a (F cm^{-2}) is the area specific capacitance, C_m (F g^{-1}) is the mass specific capacitance, I (A), Δt (s), ΔV (V), S (cm^2) and m (g) represent the constant discharging current, the discharge time, the potential window, the surface area and the mass of the electrode. Notice that the S (cm^2) and m (g) represent the surface area and the mass of the whole devices for ASC.

In order to get the charge conservation ($q^+=q^-$), the mass of activated carbon was measured by the following equation:

$$m_{\mathrm{Ni_3S_2@CoS}}/m_{\mathrm{AC}} = C_{\mathrm{m(AC)}}\,\Delta V_{\mathrm{(AC)}}/C_{\mathrm{m(Ni_3S_2@CoS)}}\Delta V_{\mathrm{Ni_3S_2@CoS}} \quad (3)$$

where C_m (F g^{-1}) is mass specific capacitance and ΔV is the potential window range for the charge-discharge process in three-electrode test system.

The equations given below were used to calculate the energy density and power density of ASC devices:

$$E = C_{\mathrm{m}}\Delta V^2/2 \quad (4)$$

$$P = E/\Delta t \quad (5)$$

Where C_m (F g^{-1}) is mass specific capacitance of ASC devices, ΔV (V) is the voltage window of ASC devices, E (Wh kg^{-1}) is the energy density, and P (W kg^{-1}) is the power density.

3. Results and discussion

Scheme 1 illustrates the two-step growth process of Ni_3S_2@CoS core-shell NTP arrays on Ni foam. Initially, Ni_3S_2 NTP arrays on Ni foam were prepared through a hydrothermal process. Subsequently, the CoS sheets were electrodeposited on the surface of Ni_3S_2 NTP arrays.

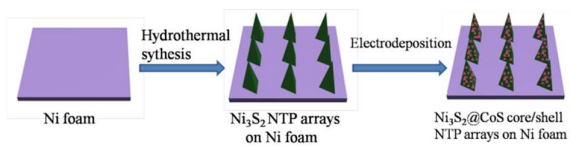

Scheme 1 a schematic illustration of a two-step process of Ni3S2@CoS core-shell NTP arrays on Ni foam.

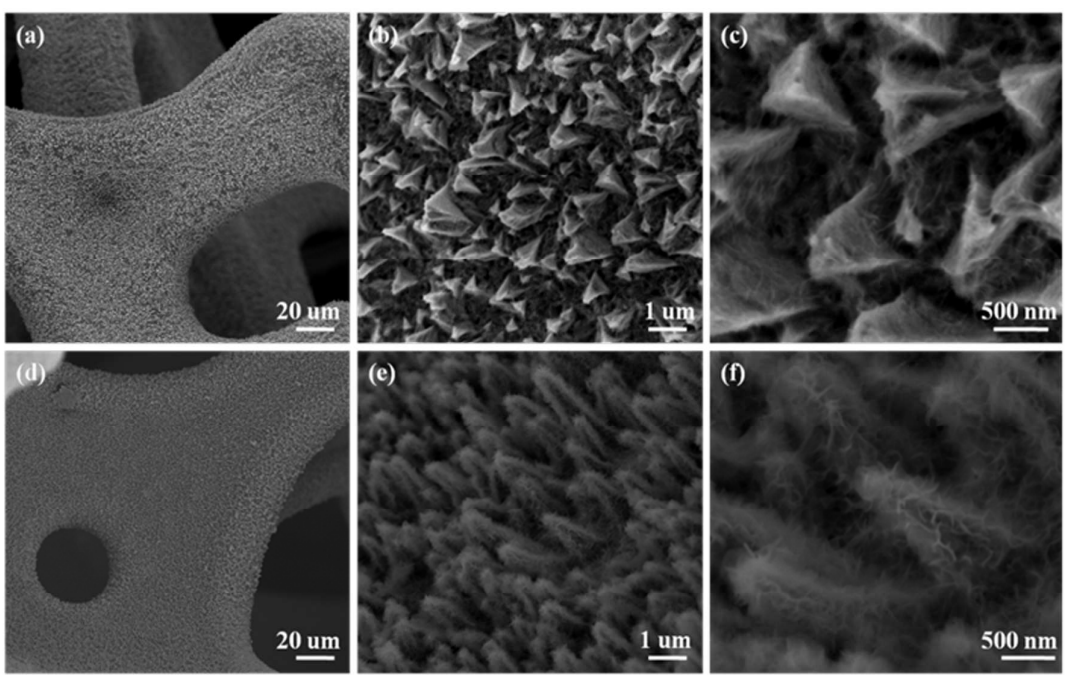

Fig. 1 FESEM images of (a-c) Ni_3S_2 NTP arrays; FESEM images of (d-f) Ni_3S_2@CoS core–shell NTP arrays.

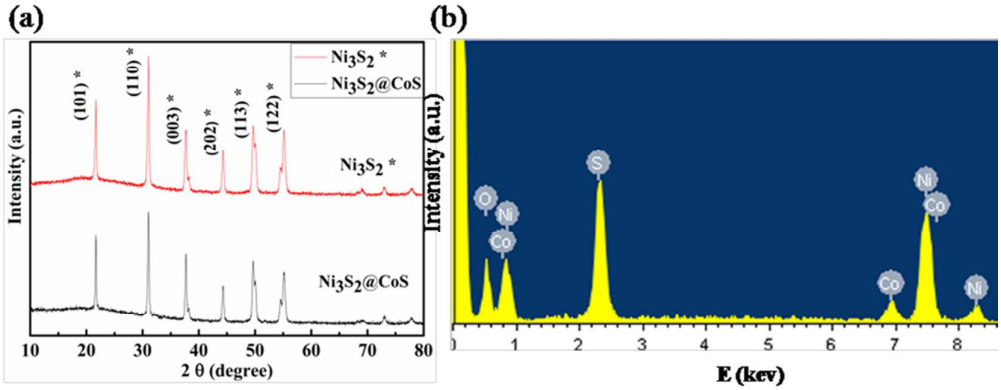

Fig. 2 (a) Powder XRD patterns of the Ni_3S_2 NTP arrays and Ni_3S_2@CoS core–shell NTP arrays; (b) EDS of Ni_3S_2@CoS core–shell NTP arrays.

Fig. 1 shows the typical micro-morphology of Ni_3S_2 NTP arrays and Ni_3S_2@CoS core-shell NTP arrays on Ni foam. As can be seen from Fig. 1 (a) and Fig. 1 (d), the Ni_3S_2 NTP arrays and Ni_3S_2@CoS core-shell NTP arrays are homogeneously distributed throughout the Ni foam on a large scale. After electrodeposited, the CoS nanosheets are coated on the surface of Ni_3S_2 NTP in Fig. 1 (b) and Fig. 1 (e). Fig. 1 (c) and Fig. 1 (f) show that CoS sheets possess highly porous structure composed of vertical interlaced nanosheets, cycling a large number of open channels, and the half-height width of each Ni_3S_2 NTP and Ni_3S_2@CoS core-shell NTP arrays is around 500 nm. Thanks to unique hierarchical core-shell structure, the diffusion pathways of electrons and ions could be shortened by the ordered gaps between NTP and vertical interlaced and ultrathin nanosheets, and also the active material could fully contact with electrolyte.

XRD was applied to analyze the different phases of the composites. In this study, to avoid the effects of the Ni foam, the samples were separated from the Ni foam (the Powder XRD patterns of samples without scrapping can be found in Fig. S2). As shown in Fig. 2 (a), the major peaks at $2\theta = 21.7°$, 31.1°, 37.7°, 44.3°, 49.7° and 55.1° correspond to the (101), (110), (003), (202), (113) and (122) planes of Ni_3S_2 (JCPDS44-1418), respectively. However, there is almost no difference between the XRD patterns of Ni_3S_2@CoS and Ni_3S_2, which can be attributed to the low mass loading and the weak crystallize of CoS nanosheets.[29-31] Nevertheless, the elements of Co and S can be detected by EDS analysis (Fig. 2 (b)), and the presence of the CoS structure could be further proved by the following XPS and TEM analysis.

To identify the chemical compositions of the shell, XPS were carried out to detect Co element on the surface of samples. As indicated in Co 2p spectra (Fig. 3), the main peak located at lower binding energy with a value of 780.2 eV and a shake-up feature was captured at high binding energy, corresponding to the characteristics of Co^{2+} in CoS on the basis of previous reports.[28, 30, 31]

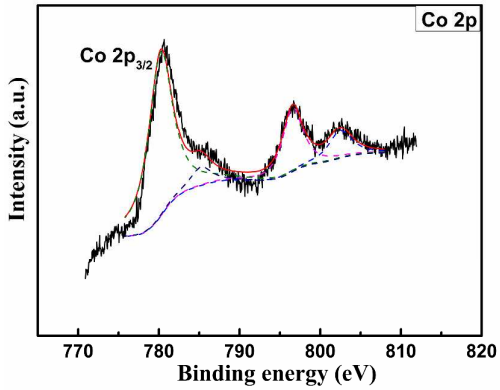

Fig. 3 XPS spectra of Co 2p

As shown in Fig. 4 (a), the core-shell structure of Ni_3S_2@CoS can be clearly observed, in which the core of Ni_3S_2 core is tightly enwrapped in the CoS nanosheets shell. Fig. 4 (b) and Fig. 4 (c) are HRTEM of core Ni_3S_2 and shell CoS. The selected area electron diffraction (SAED) pattern of Ni_3S_2@CoS core-shell NTP arrays in the inset of Fig. 4 (a) illustrates the faint diffraction rings and

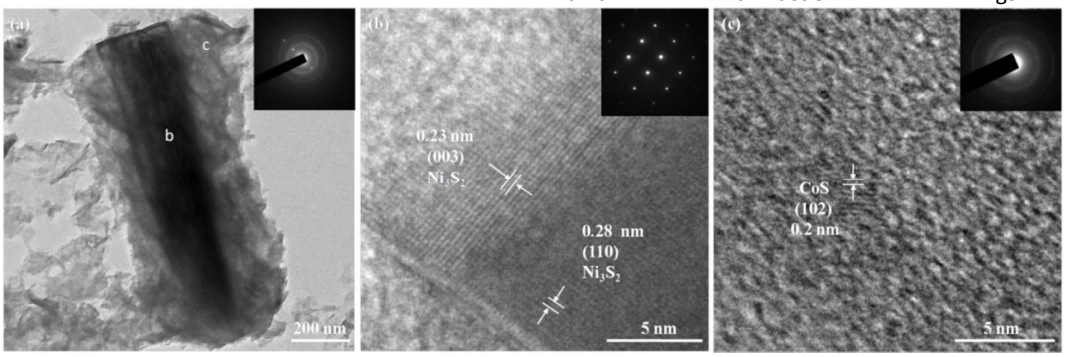

Fig. 4 (a) HRTEM images of Ni_3S_2@CoS core–shell NTP arrays; (b) HRTEM images of Ni_3S_2 NTP arrays; (c) HRTEM images of CoS NTP arrays.

Journal Name

ARTICLE

diffraction spots, suggest that the product should include two different materials. Fig. 4 (b) reflects the crystal lattices and SAED pattern of Ni_3S_2 NTP arrays. The lattice spacing of 0.23 nm corresponds to the (003) plane of Ni_3S_2, and the other lattice spacing of 0.28 nm reflects the (110) plane of Ni_3S_2. Meanwhile, the diffraction spots in SAED pattern prove that the Ni_3S_2 here is a simple crystal. Fig. 4 (c) represents a lattice spacing of 0.20 nm which can be indexed to the (102) plane of CoS with diffraction rings in the inset. In addition, both of the short crystal lattices and faint diffraction rings demonstrate that the CoS has low degree of crystallization, coincides with the deduction mentioned before. In a word, the composite possess an obvious core-shell structure proved to be composed of Ni_3S_2 NTP arrays and CoS nanosheets.

3.1. Electrochemical performance of the Ni_3S_2@CoS core-shell NTP arrays

The electrochemical properties of the products were measured in a three-electrode cell by standard cyclic voltammrtry (CV) and chronopotentiomatry (CP) measurements. Fig. 5 (a) shows the CV curves of the Ni_3S_2 NTP arrays and Ni_3S_2@CoS core-shell NTP arrays in the potential range of 0-0.6V at 5 mV s^{-1}. Clearly, Ni_3S_2@CoS core-shell NTP arrays display a larger area of CV curves than that of Ni_3S_2 NTP arrays, suggesting a higher capacitive capability of Ni_3S_2@CoS core-shell NTP arrays. The CV curves of Ni_3S_2@CoS core-shell NTP arrays at various scan rates are shown in Fig. 5 (b), a pair of redox peaks can be clearly observed around 0.45 V and 0.30 V which corresponds to the reversible reactions of Ni^{2+}/Ni^{3+}, Co^{2+}/Co^{3+} and Co^{3+}/Co^{4+}. Fig. S3 shows the cyclic voltammetry curves of the CoS electrode in 2M KOH in supporting information. From the Fig. S3, two pairs of redox peaks are observed. Notably, the potential of two redox peaks are both lower than Ni_3S_2 NTP arrays.[31] This is a main reason that contributes to the peak potential shifts after electrodepositing CoS nanosheets as shown in Fig. 5 (a). In addition, the loading of CoS nanosheets was poor and the peaks at 0.45 V and 0.3 V of Ni_3S_2@CoS NTP arrays are too strong compared with bare CoS, so that the first pair of redox peak in Fig. S3 cannot be seen apparently in Fig. 5 (a). The charge storage mechanism of Ni_3S_2 and CoS can be described as the following equations in alkaline electrolyte:[6, 31]

$$Ni_3S_2 + 3OH^- \leftrightarrow Ni_3S_2(OH)_3 + 3e^- \quad (6)$$

$$CoS + OH^- \leftrightarrow CoSOH + e^- \quad (7)$$

$$CoSOH + OH^- \leftrightarrow CoSO + H_2O + e^- \quad (8)$$

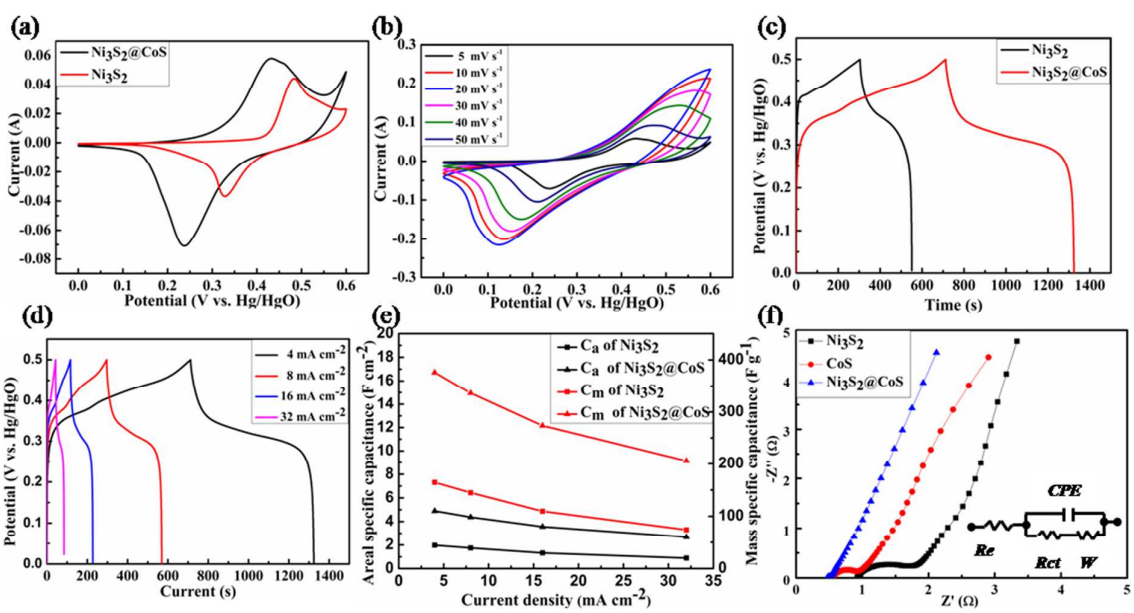

Fig. 5 (a) CV curves of the Ni_3S_2 NTP arrays and Ni_3S_2@CoS core–shell NTP arrays at 5 mV s^{-1}; (b) CV curves of Ni_3S_2@CoS core–shell NTP arrays at various scan rates; (c) Galvanostatic charge-discharge curves of the Ni_3S_2 NTP arrays and Ni_3S_2@CoS core–shell NTP arrays at 4 mA cm^{-2}; (d) Galvanostatic charge-discharge curves of Ni_3S_2@CoS core–shell NTP arrays at different current densities; (e) C_a and C_m of Ni_3S_2 NTP arrays and Ni_3S_2@CoS core–shell NTP arrays at different current densities; (f) Nyquist plots of Ni_3S_2 NTP arrays, Ni_3S_2@CoS core–shell NTP arrays and CoS in 2 M KOH solution.

Journal Name

ARTICLE

Both the equations above and the shape of CV curves prove that the Ni_3S_2 and CoS exhibit obvious pseudocapacitive behaviour, leading to higher performance of Ni_3S_2@CoS than the bare Ni_3S_2.

Fig. 5 (c) illustrates the charge-discharge curves of the Ni_3S_2 and Ni_3S_2@CoS core-shell NTP arrays in the potential range of 0~0.5V at a current density of 4 mA cm^{-2}. The charge-discharge curves and area specific capacitance of Ni_3S_2@CoS core-shell NTP arrays at different current densities are presented in Fig. 5 (d) and Fig. 5 (e) respectively. Notably, the calculated C_a value of Ni_3S_2@CoS core-shell NTP arrays is 4.89 F cm^{-2}, 4.37 F cm^{-2}, 3.56 F cm^{-2} and 2.68 F cm^{-2} (C_m : 376.06 F g^{-1}, 336.37 F g^{-1}, 273.72 F g^{-1} and 205.78 F g^{-1}) at 4 mA cm^{-2}, 8 mA cm^{-2}, 16 mA cm^{-2} and 32 mA cm^{-2} according to Eq. (1) and (2), much higher than the bare Ni_3S_2 NTP arrays with values of 1.97 F cm^{-2}, 1.74 F cm^{-2}, 1.32 F cm^{-2} and 0.89 F cm^{-2} (C_m: 164.47 F g^{-1}, 144.80 F g^{-1}, 109.60 F g^{-1} and 74.13 F g^{-1}). It's noteworthy that the obtained area specific capacitances here are higher than other core-shell structures in previous reports, such as $NiCo_2O_4$@Ni-S (1.85 F cm^{-2} at 8 mA cm^{-2}),[29] Ni@NiO (2.04 F cm^{-2} at 8 mA cm^{-2})[32] and ZnO@Co_3O_4 (1.42 F cm^{-2} at 8 mA cm^{-2}).[33]

To better understand the reaction mechanism of the Ni_3S_2@CoS core-shell NTP arrays during the charge-discharge process, the electrochemical impedance spectroscopy (EIS) measurements were performed at a frequency range from 100 kHz to 0.01 Hz. Fig. 5 (f) shows Nyquist plots of the Ni_3S_2 NTP arrays and Ni_3S_2@CoS core-shell NTP arrays. The impedance spectra exhibits a semicircle at high-frequency region and a slash shape at low-frequency region, which is commonly ascribed to charge transfer resistance and Warburg resistance, respectively. At the high-frequency region, the diameter of the semicircle of Ni_3S_2@CoS core-shell NTP arrays is smaller than that of both Ni_3S_2 and CoS, reveals a lower charge transfer resistance (R_{ct}) for Ni_3S_2@CoS core-shell NTP arrays. Besides, the real axis intercept of real part (Z') is the internal resistance (R_e), the Ni_3S_2@CoS core-shell NTP arrays reflects a smaller resistance as can be seen from Table 1. In a word, the good conductivity of Ni_3S_2@CoS core-shell NTP arrays is concluded from the structural integrity and additional electron transport path way provided by CoS nanosheets.[18] Meanwhile this good conductivity is considered as a significant factor for the high-performance in the CV and charge-discharge curves mentioned above.

Table 1 The fitted parameters of Ni_3S_2@CoS, Ni_3S_2 and CoS electrodes.

Electrode	Internal resistance (R_e/ Ω)	Charge transfer resistance (R_{ct}/ Ω)	Diffusive resistance (W/ Ω)
Ni_3S_2	0.95	0.20	0.19
CoS	0.55	0.45	0.16
Ni_3S_2@CoS	0.53	0.01	0.12

3.2 Electrochemical performances of the ASC based on Ni_3S_2@CoS and activated carbon

Before assembling asymmetric supercapacitors, the electrochemical behavior of AC electrode must be tested. The AC electrode was prepared by mixing 80 wt% active materials and 10 wt% acetylene black with 10 wt% polytetrafluorene-ethylene (PTFE). A small amount of absolute ethanol was added to the mixture with ultrasonic for 20 minutes to promote homogeneity. After that, the mixture was pressed into films and dried at 60 °C overnight. Thus it was convenient to cut it into pieces to match the weight.

As shown in Fig. 6 (a), the CV curve of the AC within a voltage window of -1.0 to 0 V exhibits a typical capacitive behavior with a nearly rectangular shape, indicating a EDLCs behavior. Therefore the whole voltage window of Ni_3S_2@CoS//AC ranges from 0 to 1.6 V owing to the combination of pseudocapacitance and EDLCs.[34, 35] Fig. 6 (a)

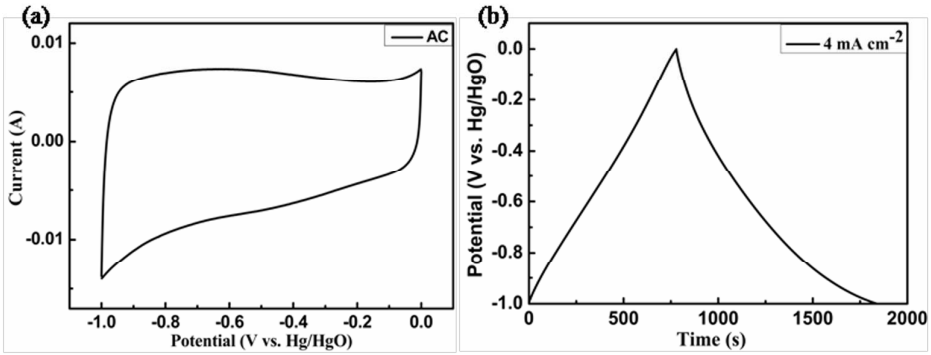

Fig. 6 (a) CV curves of the AC at 5 mV s-1; (b) Galvanostatic charge-discharge curves of the AC at different current 4 mA cm^{-2}

illustrates the charge-discharge curves of the AC at current density of 4 mA cm^{-2}. And the calculated C_m value of the AC electrode was 270 F g^{-1}. According to Eq. (3), the mass of AC in Ni_3S_2//AC and Ni_3S_2@CoS//AC were 9.5 mg and 10.8 mg, respectively.

Asymmetric supercapacitors were assembled based on Ni_3S_2@CoS cathodes, AC anodes and 2 M KOH aqueous electrolyte to further evaluate the actual application of Ni_3S_2@CoS core-shell NTP arrays in supercapacitor. The Ni_3S_2//AC device was also fabricated for comparison.

The electrochemical performances of the ASC devices were consistent with the three-electrode test results. The acreage enclosed by the CV curves of the Ni_3S_2@CoS//AC device with a voltage window of 0~1.6 V is apparently larger than that of Ni_3S_2//AC device according to Fig. 7 (a) and Fig. 7 (b). This result was also confirmed by the galvanostatic charge-discharge measurements. As shown in Fig. 7 (c), the discharge time of Ni_3S_2@CoS//AC device is about triple than the bare Ni_3S_2//AC device at 1.43 mA cm^{-2}, indicating a better electrochemical behaviour for the Ni_3S_2@CoS//AC device. Fig. 7 (d) describes the charge-discharge curves of Ni_3S_2@CoS//AC device at different current densities while Fig. 7 (e) illustrates the C_a and C_m of Ni_3S_2//AC and Ni_3S_2@CoS//AC devices. The C_a of Ni_3S_2//AC and Ni_3S_2@CoS//AC devices were calculated to be 0.68 F cm^{-2} (79.42 F g^{-1}) and 0.22 F cm^{-2} (28.16 F g^{-1}) at 1.43 mA cm^{-2}. Fig. 7 (e) displays a dramatically capacitance decrease due to the larger mass of Ni_3S_2@CoS//AC. However, the capacitance was still 0.34 F cm^{-2} (40.5 F g^{-1}) at 11.44 mA cm^{-2}, higher than that of the Ni_3S_2//AC (0.13 F cm^{-2} and 17.21 F g^{-1} at 11.44 mA cm^{-2}).

To evaluate the energy storage properties of theNi_3S_2@CoS based device, a Ragone plot (energy density versus average power density) is presented in Fig. 7 (f). The calculated energy density and power density of Ni_3S_2@CoS//AC (28.24 Wh kg^{-1} at 134.46 W kg^{-1}) are higher than that of the Ni_3S_2//AC (10.01 Wh kg^{-1} at 150.12 W kg^{-1}). Moreover, Ni_3S_2@CoS//AC ASC can maintain a well energy density with the increase of the power density (23.69 Wh kg^{-1}, 18.40 Wh kg^{-1} and 14.4 Wh kg^{-1} at 268.95 W kg^{-1}, 537.66 W kg^{-1} and 1075.52 W kg^{-1}). Furthermore, Ni_3S_2@CoS//AC also show much higher energy density than other previously reports ASCs, such as those of $NaMnO_2$//AC (19.5 Wh kg^{-1} at a power density of 130 W kg^{-1}),[36] Ni-Co oxides//AC (10.8 Wh kg^{-1} at a power density of 474.4 kg^{-1})[37] and Mn_3O_4@GR//AC (13.5 Wh kg^{-1} at a power density of

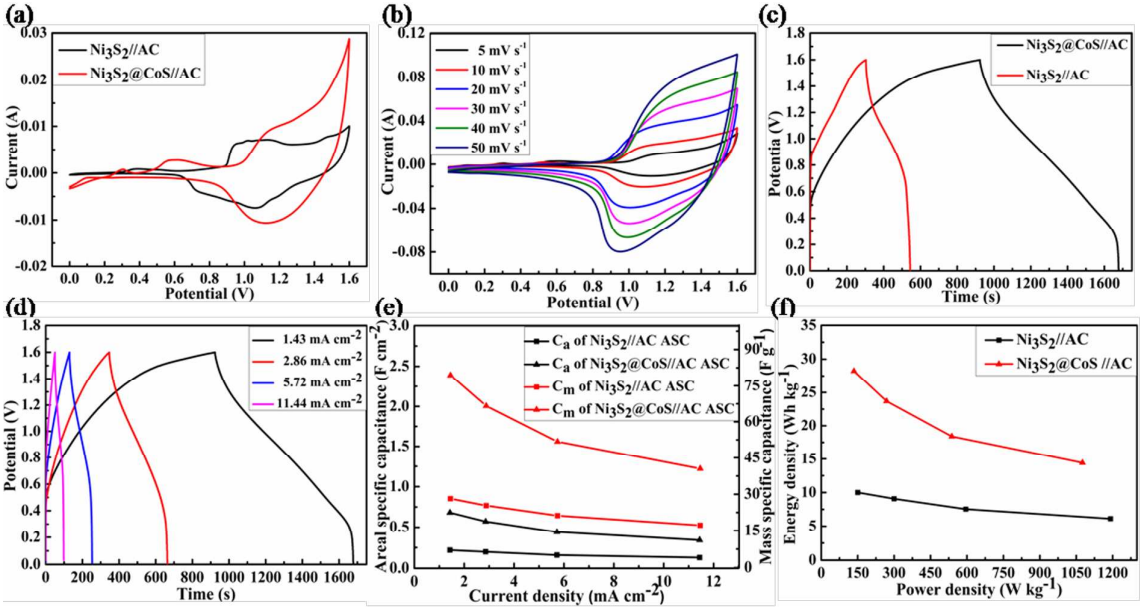

Fig. 7 (a) CV curves of the Ni_3S//AC and Ni_3S_2@CoS//AC at 5 mV s^{-1}; (b) CV curves of Ni_3S_2@CoS//AC at various scan rates; (c) Galvanostatic charge-discharge curves of the Ni_3S//AC and Ni_3S_2@CoS//AC at 1.43 mA cm^{-2}; (d) Galvanostatic charge-discharge curves of Ni_3S_2@CoS//AC at different current densities; (e) C_a and C_m of Ni_3S_2//AC and Ni_3S_2@CoS//AC at different current densities; (f) Ragone plots of energy density and power density of Ni_3S_2// AC and Ni_3S_2@CoS//AC.

400 W kg^{-1}).[38] The superior energy density and power density of Ni_3S_2@CoS//AC is ascribed to the synergy effect resulting from the more active states for the Faradaic reactions provided by CoS nanosheets.

Fig. 8 shows the long term cycle life of Ni_3S_2//AC and Ni_3S_2@CoS//AC with consecutive galvanostatic charge-discharge experiment for 2000 cycles at 5.72 mA cm^{-2} in a LAND battery test system. The specific capacitance of ASC devices increase gradually and remain stable after 800 cycles. This large increase mainly resulted from the activation of the active materials in the first 800 cycles. Especially, the mass loading of ASC devices was so large that it took some time to activate the electrodes. The similar experiments results can be confirmed from many other studies, such as: Ref. 9, Ref. 18

and Ref. 29. And the corresponding appropriate explanations were given in revised manuscript. As illustrated in Fig. 8, both Ni_3S_2 //AC and Ni_3S_2@CoS//AC display long cycle lives with a capacitance loss of only 1.17% and 4.41% after 2000 cycles due to their good conductivity and strong adherence with the substrate.

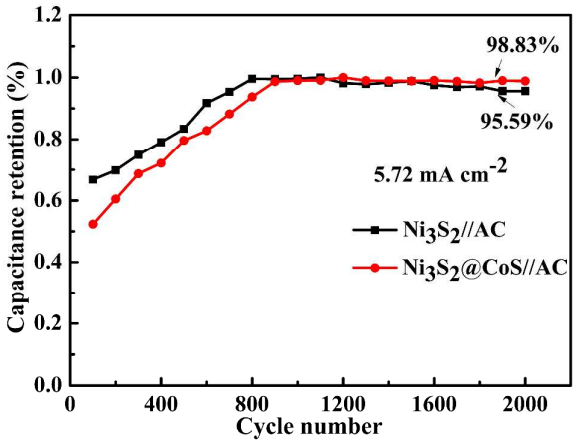

Fig. 8 long term cycle life graph of Ni_3S_2//AC and Ni_3S_2@CoS//AC.

The enhanced properties of Ni_3S_2@CoS core-shell NTP arrays are mainly owe to their unique core-shell structure on Ni foam that includes the following advantages. (1) Both Ni_3S_2 and CoS are good electrode materials for pseudocapacitors, hence contributing to the enhanced capacitance activity. (2) Ni_3S_2 and Ni_3S_2@CoS core-shell NTP arrays can be conveniently used as bind-free electrodes that can avoid interferences from some binding materials. (3) The heazlewoodite Ni_3S_2 with short Ni-Ni distances, resulting in allowing good metallic conduction and enabling the quick transfer of ions and electrons along the Ni_3S_2 NTP arrays.[24, 39, 40] (4) The Ni_3S_2 NTP arrays form from sulfuration of the Ni foam and CoS nanosheets firmly electroposited on the surface of Ni_3S_2 NTP arrays, maintaining a core-shell structure with great chemical and mechanical stabilities. (5) The ordered void between Ni_3S_2 NTP and the space of neighboring CoS nanosheets are beneficial to fast electron transfer and ion diffusion, which greatly improve charge-discharge rate and reactivity.[41-43] In summary, the product of Ni_3S_2@CoS core-shell NTP arrays on Ni foam is a potential candidate for supercapacitors, and the unique template of Ni_3S_2 NTP arrays is suitable for other core-shell structures.

4. Conclusions

In this paper, the Ni_3S_2 and Ni_3S_2@CoS core-shell NTP arrays have been successfully synthesized by two steps including the hydrothermal and electrodepositing process. The obtained Ni_3S_2@CoS core-shell NTP arrays reflect amazing electrochemical performances with a high C_a value of 4.89 F cm^{-2} at 4 mA cm^{-2} in three-electrode cell, a well C_a value of 0.69 F cm^{-2} (79.42 F g^{-1}) at 1.43 mA cm^{-2} in ASC, an outstanding energy density of 28.24 Wh kg^{-1} at a power density of 134.46 W kg^{-1} and a stable long cycle life of 1.17% lost after 2000 cycles. Thus, Ni_3S_2@CoS core-shell NTP arrays on Ni foam are promising and attractive in application of supercapacitors based on its high C_a capacitance, good conductivity and excellent long cycle life. Moreover, the Ni_3S_2 NTP arrays can also be applied in template-based method to fabricate a variety of composites so as to improve the performance of materials.

Acknowledgements

The authors would like to acknowledge testing support from the Analysis and Testing Center, Xiamen University.

Notes and references

1 P. Simon and Y. Gogotsi, *Nat.Mater.*, 2008, 7, 845-854.
2 P. J. Hall, M. Mirzaeian, S. I. Fletcher, F. B. Sillars, A. J. Rennie, G. O. Shitta-Bey, G. Wilson, A. Cruden and R. Carter, *Energy Environ. Sci.*, 2010, 3, 1238-1251.
3 C. Liu, Z. Yu, D. Neff, A. Zhamu and B. Z. Jang, *Nano Lett.*, 2010, 10, 4863-4868.
4 M. R. Gao, Y. F. Xu, J. Jiang and S. H. Yu, *Chem. Soc. Rev.*, 2013, 42, 2986-3017.
5 L. Yui, N. N. Shi, Q. Liu, J. Wang, B. Yang, B. Wang, H. J. Yan, Y. B. Sun and X. Y. Jing, *Phys. Chem. Chem. Phys.*, 2014, 16, 17936-17942.
6 K. Krishnamoorthy, G. K. Veerasubramani, S. Radhakrishnan and S. J. Kim, *J. Power Sources*, 2014, 251, 116-122.
7 J. Jiang, Y. Y. Li, J. P. Liu, X. T. Huang, C. Z. Yuan and X. W. Lou, *Adv. Mater.*, 2012, 24, 5166-5180.
8 M. E. Roberts, D. R. Wheeler, B. B. McKenzie and B. C. Bunker, *J. Mater. Chem.*, 2009, 19, 6977-6979.
9 Z. C. Huang, S. L. Wang, J. P. Wang, Y. M. Yu, J. J. Wen and R. Li, *Electrochim. Acta*, 2015, 152, 117-125.
10 M. J. Zhi, C.C Xiang, J. T. Li, M. Li and N. Q. Wu, *Nanoscale*, 2013, 5, 72-88.
11 V. Sozolins, F. Zhou and M. Asta, *Accounts Chem. Res.*, 2013, 46, 1084-1093.
12 G. A. Snook, P. Kao and A. S. Best, *J. Power Sources*, 2011, 196, 1-12.
13 C. H. Lai, M.Y. Luand and L.J. Chen, *J. Mater. Chem.*, 2012, 22, 19-30.
14 S. L. Shen and Q. B. Wang, *Chem. Mater.*, 2013, 25, 1166-1178.
15 X. H. Rui, H. T. Tang and Q. Y. Yan, *Nanoscale*, 2014, 6, 9889-9924.
16 Z. C. Xing, Q. X. Chu , X. B. Ren, J. Q. Tian, Abdullah M. Asiri, Khalid A. Alamry, Abdulrahman O. Al-Youbi and X. P. Sun, *Electrochem. Commun.*, 2013, 32, 9-13.
17 Z. C. Xing, Q. X. Chu , X. B. Ren, C. J. Ge, Abdullah H. Qusti, Abdullah M. Asiri Abdulrahman O. Al-Youbi, and X. P. Sun, *J. Power Sources*, 2014, 245, 463-467.
18 J. P. Wang, S. L. Wang, Z. C. Huang and Y. M. Yu, *J. Mater. Chem.*, 2014, A2, 17595-17601.
19 M. Huang, F. Li, X. L. Zhao, D. Luo, X. Q. You, Y. X. Zhang and G. Li, *Electrochim. Acta*, 2015, 152, 172-177.
20 L. Gu, Y. W. Wang, R. Lu, W. Wang, X. S. Peng and J. Sha, *J. Power Sources*, 2015,273, 479-485.
21 K. W. Qiu, Y. Lu, D. Y. Zhang, J. B. Cheng, H. L. Yan, J. Y. Xu, X. M. Liu, J. K. Kim and Y. S. Luo, *Nano Energy*, 2015, 11, 687-696.
22 W. J. Zhou, X. J. Wu, X. H. Cao, X. Huang, C. L. Tan, J. Tian, H. Liu, J. Y. Wang and H. Zhang, *Energy Environ. Sci.*, 2013, 6, 2921-2924.

23 W. Wei, L. W. Mi, Y. Gao, Z. Zheng, W. H. Chen and X. X. Guan, *Chem. Mater.*, 2014, 26, 3418-3426.
24 W. J. Zhou, X. H. Cao, Z. Y. Zeng, W. H. Shi, Y. Y. Zhu, Q. Y. Yan, H. Liu, J. Y. Wang and H. Zhang, *Energy Environ. Sci.*, 2013, 26, 2216-2221.
25 F. Tao, Y. Q. Zhao, G. Q. Zhang and H. L. Li, *Electrochem. Commun.*, 2007, 9, 1282-1287.
26 Q. H. Wang, L. F. Jiao, H. M. Du, J. Q. Yang, Q. N. Huan, W. X. Peng, Y. C. Si, Y. J. Wang, H. T. Yuan, *CrystEngComm*, 2013, 13, 6960-6963.
27 M. K. Wang, A. M. Anghel, B. Marsan, N. C. Ha, N. Pootrakulchote, S. M. Zakeeruddin and M. Gratzel, *J. Am. Chem. Soc.*, 2009, 131, 15976-15977.
28 J. Y. Lin, J. H. Liao and S. W. Chou, *Electrochim. Acta*, 2011, 56, 8818-8826.
29 Q. X. Chu, W. Wang, X. F. Wang, B. Yang, X. Y. Liu and J. H. Chen, *J. Power Sources*, 2015, 276, 16-25.
30 Y. J. Sun, C. Liu, D. C. Grauer, J. Yano, J. R. Long, P. D. Yang and C. J. Chang, *J. Am. Chem. Soc.*, 2013, 135, 17699-17702.
31 J. Y. Lin and S. W. Chou, *RSC Adv.*, 2013, 3, 2043-2048.
32 M. Y. Yu, W. Wang, C. Li, T. Zhai, X. H. Luand and Y. X. Tong, *NPG Asia Mater.*, 2014, 6, e129.
33 D. P. Cai, H. Huang, D. D. Wang, B. Liu, L. L. Wang, Y. Lin, Q. H. Li and T. H. Wang, *ACS Appl. Mater. Inter.*, 2014, 6, 15905-15912.
34 C. Z. Yang, M. Z. and Q. Xu, *Phys. Chem. Chem. Phys.*, 2013, 15, 19730-19740.
35 Y. Z. Su, K. Xiao, N. Li, Z. Q. Liu and S. Z. Qiao, *J. Mater. Chem. A*, 2014, 2, 13845-13853.
36 Q. T. Qu, Y. Shi, S. Tian, Y. H. Chen, Y. P. Wu and R. Holze, *J. Power Sources*, 2009, 194, 1222-1225.
37 C. H. Tang, Z. Tang and H. Gong, *J.Electrochem.soc.*, 2012, 159, A651-A656.
38 Y. H. Xiao, Y. B. Cao, Y. Y. Gong, A. Q. Zhang, J. H. Zhao, S. M. Fang, D. Z. Jia and F. Li, *J. Power Sources*, 2014, 246, 926-933.
39 A. N. Buclley, R. Woods, *J. Appl. Electrochem.*, 1991, 21, 575-582.
40 Z. W. Lu, B. M. Klein, D. J. Singh, *Phys. Rev. B,* 1996, 54, 13542-13545.
41 J. Pu, Z. H. Wang, K. L. Wu, N. Yu and E. H. Sheng, *Phys. Chem. Chem. Phys.*, 2014, 16, 785-791.
42 J. J. Shao, X. Y. Zhou, Q. Liu, R. J. Zou, W. Y. Li, J. M. Yang and J. Q. Hu, *J. Mater. Chem. A,* 2015, 3, 6168–6176.
43 M. Kim and J. Kim, *Phys. Chem. Chem. Phys.*, 2014, 16, 11323-11336.